

The Upper San Fernando Dam

1 Background

There was a significant earthquake in Southern California in 1971, which is referred to as the San Fernando earthquake. The earthquake occurred on February 9, 1971 at 6:00 a.m. local time and had a 6.6 Richter magnitude.

The earthquake created a liquefaction failure at a water storage facility known as the Lower San Fernando Dam and Reservoir in the San Fernando community on the northern edge of the greater metropolitan Los Angeles area. Another facility known as the Upper San Fernando Dam also suffered some damage, but it was not as serious as at the Lower Dam.

Figure 1 shows an aerial view of the area. The Lower Dam is on the left side of the picture and the Upper Dam is towards the upper right of the picture. US Interstate Freeway 5 is on the right of the picture.



Figure 1 The San Fernando dams and reservoirs

The earthquake shaking initiated a major failure on the upstream side of the dam. The photos in Figure 2, Figure 3 and Figure 4 show some of the conditions after the earthquake. Of significance is the very steep slide head scarp (Figure 2) and very marginal freeboard that remained after the failure.

These photos are from Professor Ross W. Boulanger's web site photo album at the University of California, Davis, California. The web site link is:

<http://cee.engr.ucdavis.edu/faculty/boulanger/>

Presumably, based on the names on the photographs, they were taken by H.B. (Harry) Seed and J.M. (Mike) Duncan.

The failure led to a perilously close catastrophe. Had the head scarp been slightly lower, the outflow from the reservoir would have quickly eroded the dam and flooded many communities downstream. Considering the extremely precarious situation, some 80,000 people over an 11-square-mile area were evacuated while the reservoir was emptied over a period of three to four days.



Figure 2 Upstream face of the dam after the drawing down the reservoir



Figure 3 General view of the slide head scarp



Figure 4 A close-up view of the slide head scarp

2 Case history

The San Fernando dams have become extremely important case histories for geotechnical earthquake engineering. Due to their significance, the cases have become the subject of years of research and numerous publications.

Much of the early research was done by Professor H. Bolton (Harry) Seed and his colleagues at the University of California at Berkeley. Their work led to three papers, which provide much of the background information and early investigation findings. The three papers are:

Seed, H.B., Lee, K.L., Idriss, I.M. and Makadisi, F.I. (1975). *The Slides in the San Fernando Dams during the Earthquake of February 9, 1971* – ASCE, J of the Geotechnical Engineering Division, GT7, pp. 651-688

Lee, K.L., Seed, H.B., Idriss, I.M., and Makadisi, F.I. (1975). *Properties of Soil in the San Fernando Hydraulic Fill Dams* – ASCE, J of the Geotechnical Engineering Division, GT8, pp. 801-821

Seed, H.B., Idriss, I.M., Lee, K.L. and Makadisi, F.I. (1975). *Dynamic Analysis of the Slide in the Lower San Fernando Dam during the Earthquake of February 9, 1971* – ASCE, J of the Geotechnical Engineering Division, GT9, pp. 889-911

Reference to these papers will be made as Seed et al. throughout this document. These papers were published in three consecutive months; July, August and September.

3 Purpose

In light of the importance of the San Fernando Dam case histories and their prominence in the literature, it is important to show how GeoStudio, and in particular QUAKE/W, can be used to analyze cases like this. This example concentrates on the Upper Dam.

The purpose here is not to replicate all that has been done by others, or to necessarily adopt the exact conditions presented by others, but to more generally illustrate the features and capabilities of GeoStudio in the context of a famous case history.

The emphasis here is on QUAKE/W because the cases involve earthquake shaking, but SEEP/W, SLOPE/W and SIGMA/W are also used for various aspects of the analysis.

4 Design and construction

The following diagram shows a sketch of the Upper San Fernando Dam. The dam was constructed directly on the native streambed alluvium. The main body of the dam was constructed by what is known as a semi-hydraulic fill method. The material was hauled to the site by wagons and dumped into a pond where it was dispersed by water jets operating from barges. Although there is no mention of it in the publications, this technique must have created an outer shell of material compacted to some degree by the construction traffic. The material for this portion of the dam was obtained from the valley floor.

The hydraulic fill method was used up to El. 1200 feet (365 m) and then was topped-off with compacted fill to El. 1218 (371 m). This resulted in a 100-foot berm on the downstream side.

The conditions in the downstream toe area are not well known. Seed et al. make the comment that, *the soil in this area consisted of about 8 ft (2.4) of loose silty sandy fill overlying alluvium. The origin, date, and method of placing this fill are unknown.*

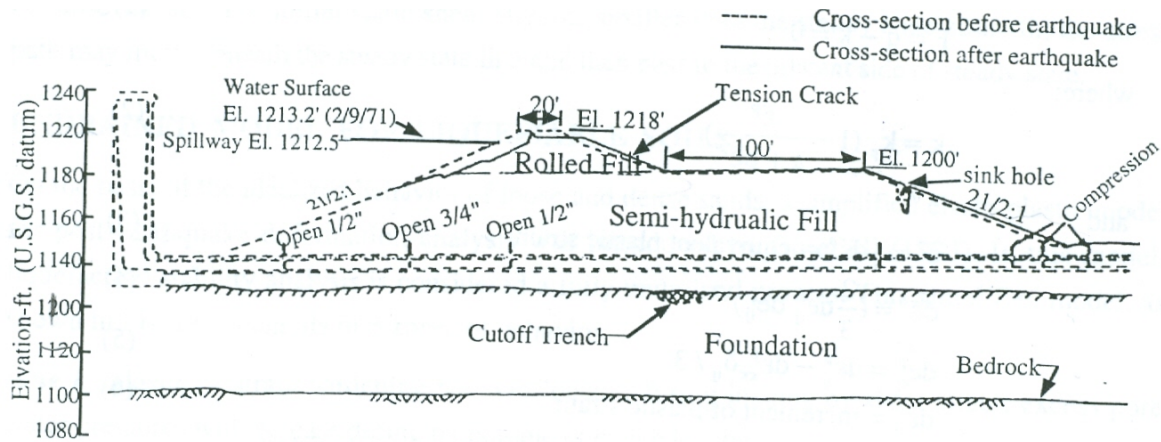


Figure 4 Cross-section through Upper San Fernando Dam (1 ft = 0.305 m) [modified after L. A. Dept. of Water and Power].

Figure 5 Sketch of the Upper San Fernando Dam

5 Effects of the earthquake

Surveys taken after the earthquake revealed that the entire upper portion of the dam had moved downstream around 2 m and the crest had moved downward around three-quarters of a meter. Based on the sketch in Figure 5, only the upper rolled-fill portion moved on the upstream side. Of significance is the movement along the surface of the berm. Here, the movements were predominantly in the lateral direction with hardly any settlement.

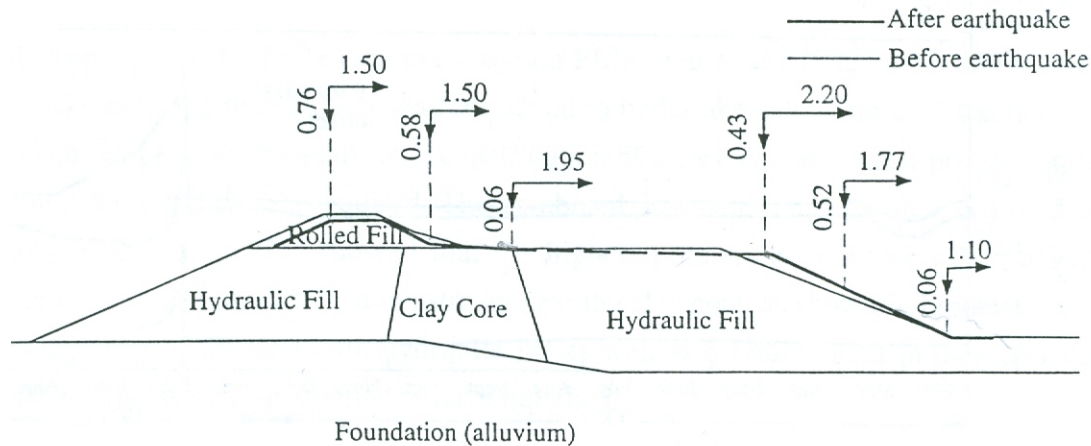


Figure 6 Movements associated with the earthquake

There were three piezometers in the dam, as shown in Figure 7. As indicated by the piezometric records, there was a sudden and dramatic increase in pore-pressures. Even 24 hours after the earthquake, water was still running out of the top of Piezometers 1 and 2. This is of significance, since these piezometers are in the core area of the dam, especially Piezometer 2. The peak in Piezometer 3 was likely higher than what was measured, due to some dissipation within the 24 hours between the event and the readings. These piezometers provide definitive evidence that substantial excess pore-pressures resulted from the shaking.

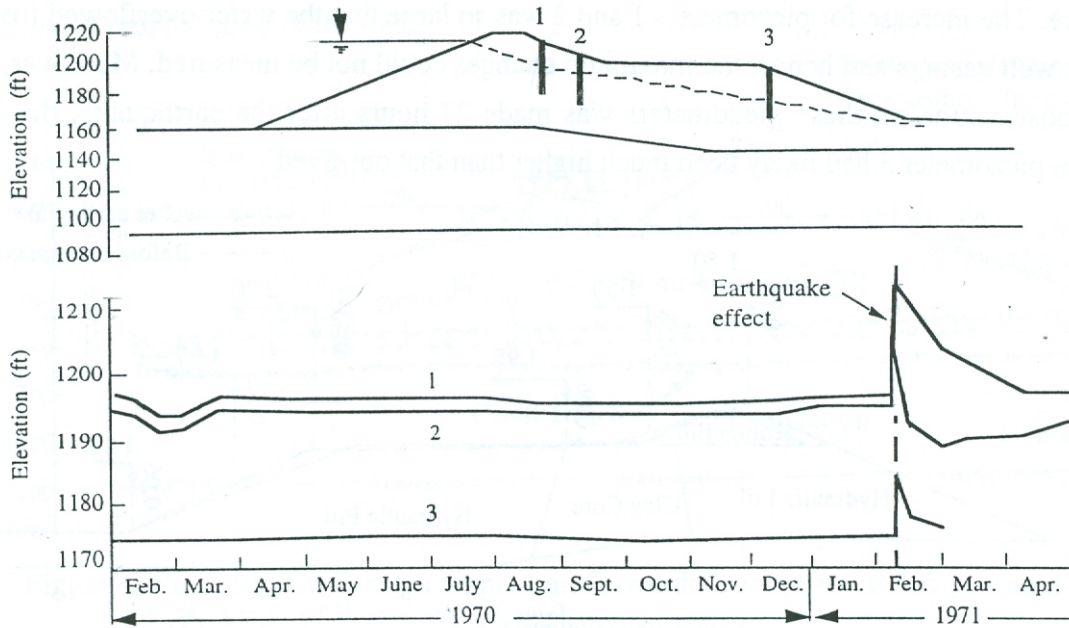


Figure 7 Piezometers and pore-pressure responses due to the shaking

The low level outlet conduit was inspected after the earthquake, and the condition of the conduit provided some interesting clues about the movement that occurred. On the upstream side, the conduit was extended as indicated by the openings noted in Figure 5. Toward the downstream toe, however, the conduit was forced into compression, as indicated by compression failures.

Also of significance is the observation that at the downstream toe a 2-foot high pressure ridge had developed and a concrete man-hole was titled and sheared in the downstream direction, indicating both lateral and upward movement.

6 Analysis configuration and setup

For the analysis here, the Upper Dam cross-section was idealized, as shown in Figure 8.

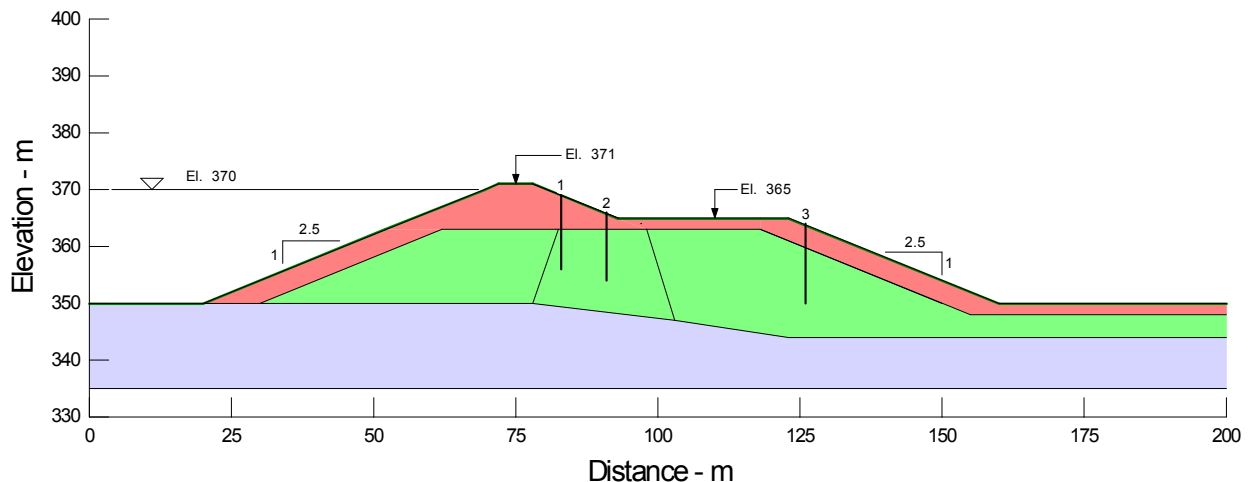


Figure 8 Numerical analysis model of the Upper San Fernando Dam

6.1 Clay core

Seed et al. present the cross-section as having a clay core. For the analysis here, the entire hydraulic fill is treated as one material. The reasons for this, as will be discussed below, is that the results this way give a picture closer to what actually happened. Furthermore, Peter Byrne in his R.M. Hardy Keynote address at the 2006 Canadian Geotechnical Conference in Vancouver suggested that stratification may have a significant impact on the potential for liquefaction. He looked at the impact of thin layers of clay amongst layers of loose sand and found that the impeded drainage resulting from the clay layers had a significant impact on the liquefaction response of the material in general. It is not difficult to imagine that there was some stratification at the Upper San Fernando Dam in the core area, especially considering the semi-hydraulic fill placement procedure used. Based on these more recent concepts, it is possible that there was some generation of excess pore-pressures and associated strength loss in the core area, just like in the remainder of the hydraulic fill. The piezometer records noted earlier strongly suggest this was indeed the case.

6.2 Soil properties

Soil properties for this analysis here are in large part estimates, filtered somewhat by values reported by Seed et al. In the end, it turns out that when stability is the main issue, these estimated values are adequate to understand the observed behavior and processes.

Generally, the streambed alluvium, outer shell, and top rolled fill are treated as somewhat more competent than the hydraulic fill.

All of the details can be viewed and examined in the associated GeoStudio data file.

7 Liquefaction and the collapse surface

Chapter 1 in the QUAKE/W Engineering Book presents a section on the Behavior of Fine Sand. This Section introduces the concept of a Collapse Surface. Figure 9 is one of the diagrams presented in Chapter 1. Fundamentally, any stress point such as Point B could experience the development of excess pore pressures during an earthquake, until the mean effective stress p' reaches the collapse surface. Once on the collapse surface, the strength may fall down to the steady-state strength. On the other hand, the initial stress Point B in Figure 10 may experience the development of excess pore-pressures, but the strength will not suddenly fall, since the initial deviatoric stress q is below the steady-state strength. This is discussed in more detail in the QUAKE/W Engineering Book.

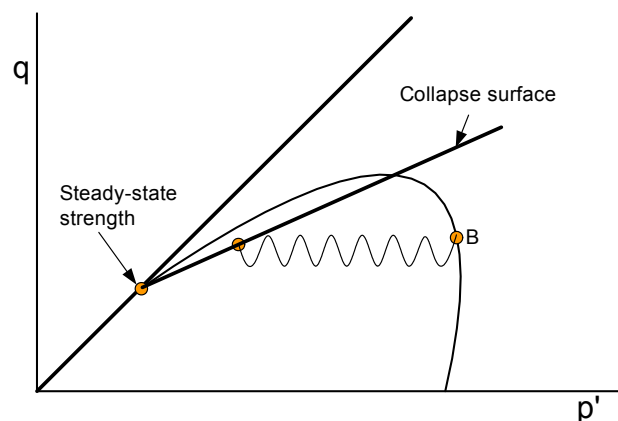


Figure 9 Stress path of contractive loose sand

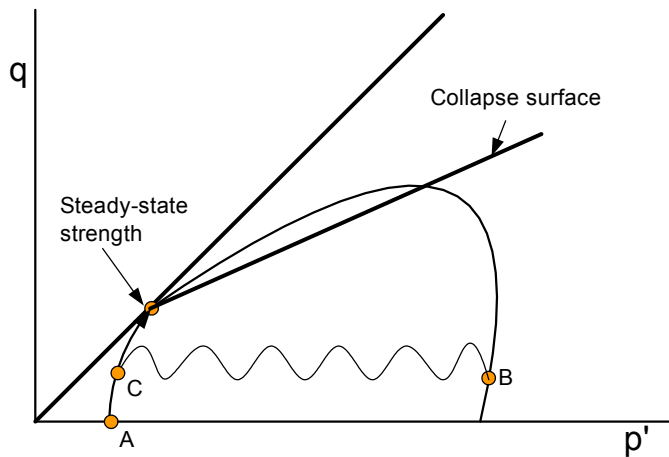


Figure 10 Stress path of dense dilative sand

QUAKE/W has an option to make use of the steady-state strength and the collapse surface to identify elements that can liquefy.

The user specifies the steady-state strength as C_{ss} and the inclination of the collapse surface.

C_{ss} is multiplied by a factor of two to define q_{ss} , the steady-state deviatoric stress.

The slope of the Critical-State Line (CSL) is computed from,

$$M_{CSL} = \frac{6 \sin \phi'}{3 - \sin \phi'} \text{ where } \phi' \text{ is the specified effective friction angle.}$$

The slope of the collapse surface is computed the same way, by substituting the specified collapse surface angle for ϕ' . In the q - p' space, we can call the slope of the collapse surface M_{CS} . Once M_{CSL} , M_{CS} and q_{ss} have been established, any q on or above the collapse surface can be computed for any p' value.

The rules adopted in QUAKE/W are as follows:

Ratios of q/p' are computed for each element using the **initial** static stresses

If q is less than q_{ss} , the element liquefaction flag is never set to “true”; excess pore-pressures can develop, but the element is not flagged as having liquefied regardless of the pore-pressures that develop

If the q/p' ratio is such that the stress state is on or above the collapse surface, the element is flagged as having liquefied even before any earthquake shaking has started, since any small amount of shaking could cause the strength to fall down to the steady-state strength

Elements with initial stress states such that q is greater than q_{ss} but the stress points under the collapse surface are initially marked as not liquefied

Stress points initially under the collapse surface will move to the left as pore-pressures develop during the shaking, and they are then marked as liquefied when the stress point is on or above the collapse surface

Excess pore pressures are limited or restricted so that the mean effective stress p' is not lower than the p' corresponding with q_{ss} on the CSL. This prevents the effective stresses from becoming too low or even negative, which in turn reduces difficulties with numerical instability (convergence).

Castro et al. (1992) did an extensive study of the steady-state strength of the Lower San Fernando Dam hydraulic fill material. They concluded that the average undrained steady-state strength was between 30 and 40 kPa depending on the method used to obtain the strength. Values in this range are used in the GeoStudio analyses presented here.

Little information is available in the literature on the slope of the collapse surface. It is definitely a value lower than the effective friction ϕ' . Kramer (1996, p. 364) suggests that an approximation is about two-thirds of ϕ' . For the analyses here, a value of 20 degrees was arbitrarily chosen, which is about 0.6 of the ϕ' (0.6×34).

8 Analysis: Initial PWP

The first step in the modeling process is to establish the long-term steady-state seepage conditions and pore-pressures. This can be done with SEEP/W. The conditions that existed in the downstream toe before the earthquake are not well known. There is no discussion in the literature about this. However, based on various sketches by others, there are suggestions that watertable was 1 to 2 meters below the ground surface. To simulate this, a Head-type boundary condition is applied along the contact between the upper crust and the underlying granular material.

Also, it is arbitrarily assumed that a piezometric surface did not exist in the outer shell above the downstream toe. To prevent this, the boundary between the outer shell and the hydraulic fill is tagged as a potential seepage face. This ensures that the pore-pressure cannot be greater than zero along this material contact line.

Approximate conductivity functions and K_{sat} values are adequate for this steady-state analysis since the piezometric surface is high up in the dam and much of the seepage flow is in the saturated zone. Also, the pore-pressure distribution, the parameter of interest here, is not sensitive to K_{sat} .

Figure 11 shows the resulting piezometric line (watertable) and total head contours (equipotential lines). Note that the piezometric line comes very close to the ground surface at the toe of the upper rolled section.

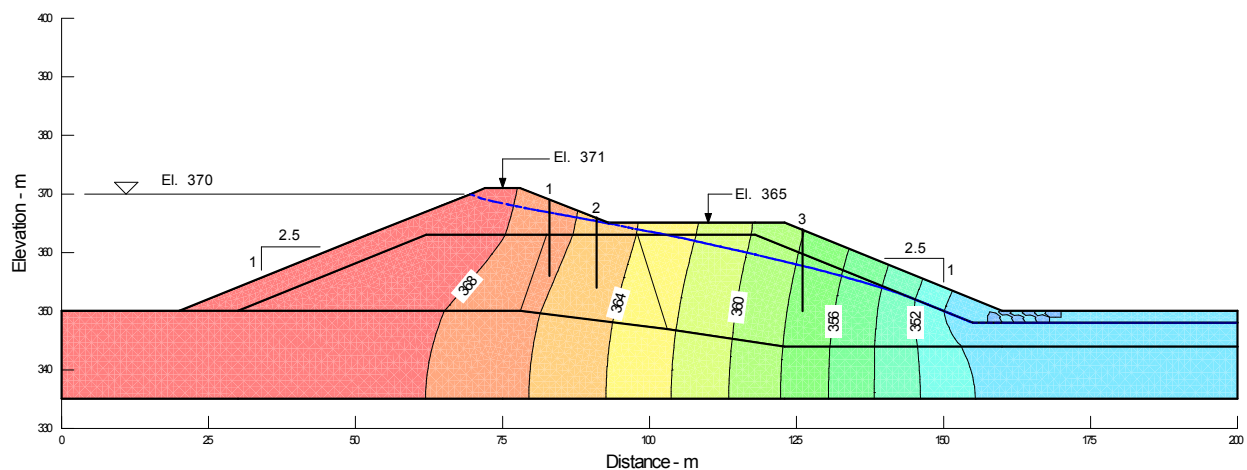


Figure 11 Long term steady-state seepage and pore-pressure conditions

9 Initial stress state

The next step is to establish the initial total and effective static stress distribution throughout the dam. This can be done with a QUAKE/W Static-type of analysis or a SIGMA/W Insitu analysis. The QUAKE/W Initial Static analysis type is used here.

To compute the initial static stresses, it is necessary to specify Poisson's ratio and the total unit weight of the soils. Remember that Poisson's ratio is used indirectly to say something about K_0 - the remainder of the specified material properties do not influence the insitu stress calculations.

The previously computed SEEP/W pore-pressures are used in the static stress analysis.

It is important to include the weight of the reservoir water in the static stress analysis. This is done by applying a fluid pressure boundary on the region edges in contact with the reservoir. This is illustrated in Figure 12. The resulting vertical effective stresses, for example, are as shown in Figure 13.

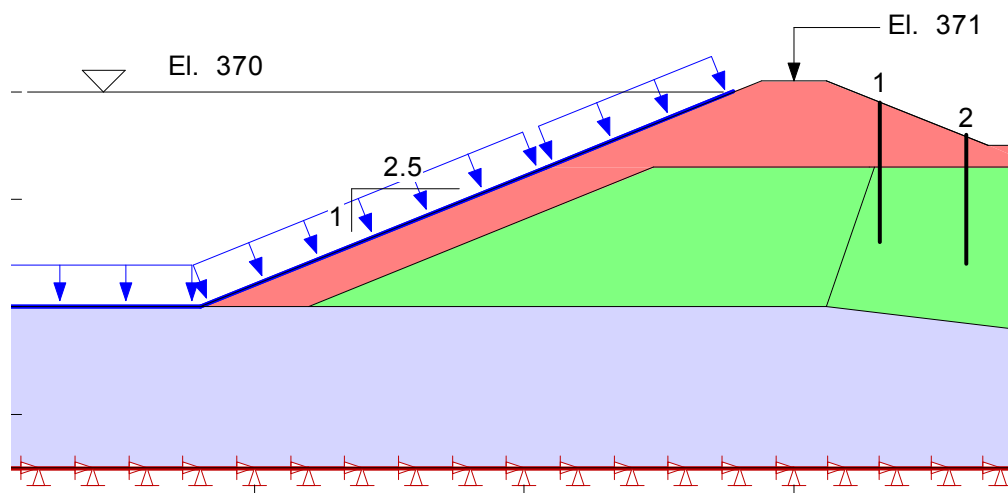


Figure 12 The reservoir water weight boundary condition

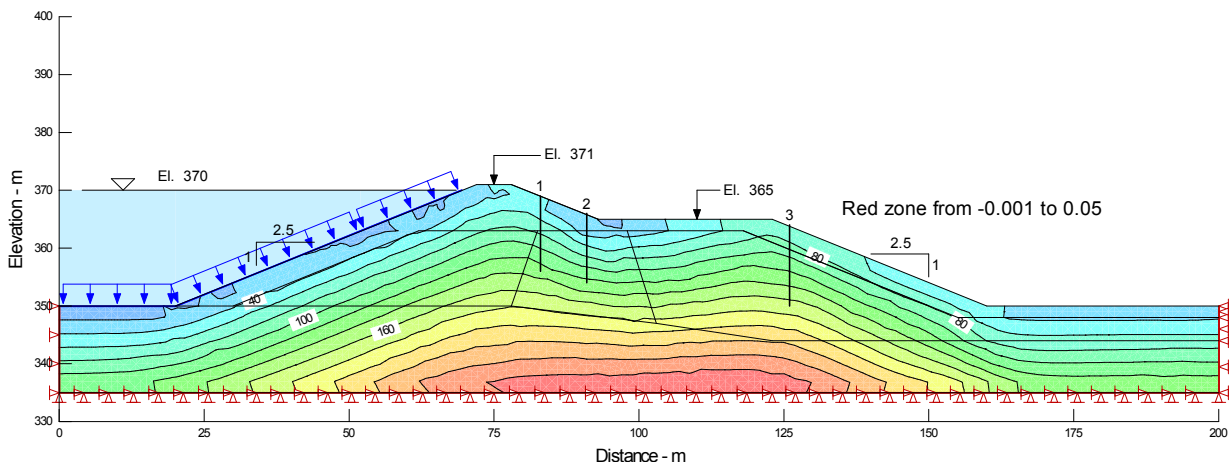


Figure 13 Initial static vertical effective stresses

10 Factor of safety under static conditions

As a reference point, it is useful to know the factor of safety under static conditions before the slide occurred. Based on the SEEP/W pore-pressures and QUAKE/W static stresses, the factor of safety is well above 2.0, as illustrated in Figure 14. This is consistent with the findings by Seed et al., who concluded that the margin of safety against instability under the static conditions was fairly high.

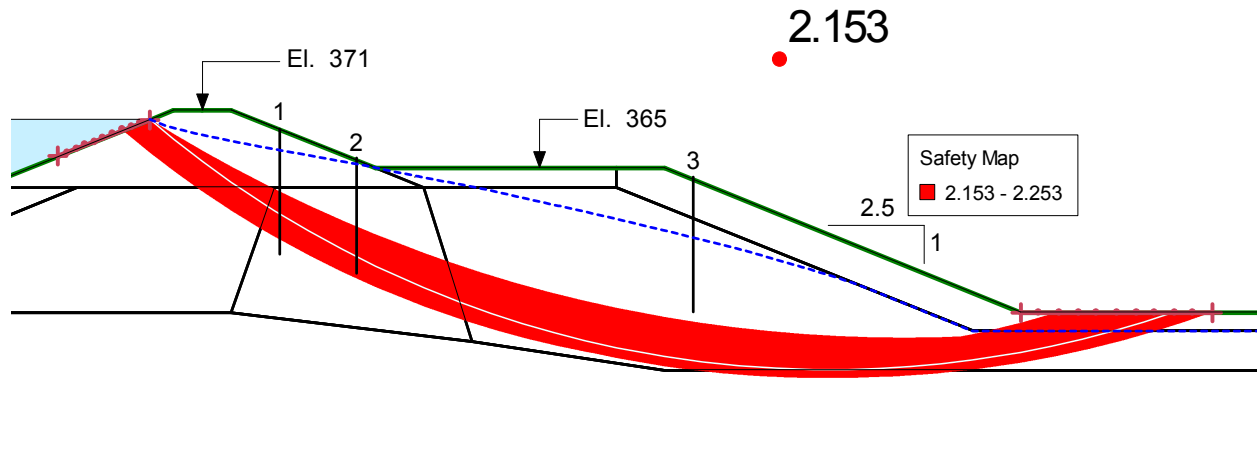


Figure 14 Overall margin of safety before the earthquake

The safety factor of the downstream slope of the hydraulic fill section is shown in Figure 15. As with the overall factor of safety, the factor of safety for this potential mode of failure is also fairly high. The factor of safety in the red band is between 1.70 and 1.80.

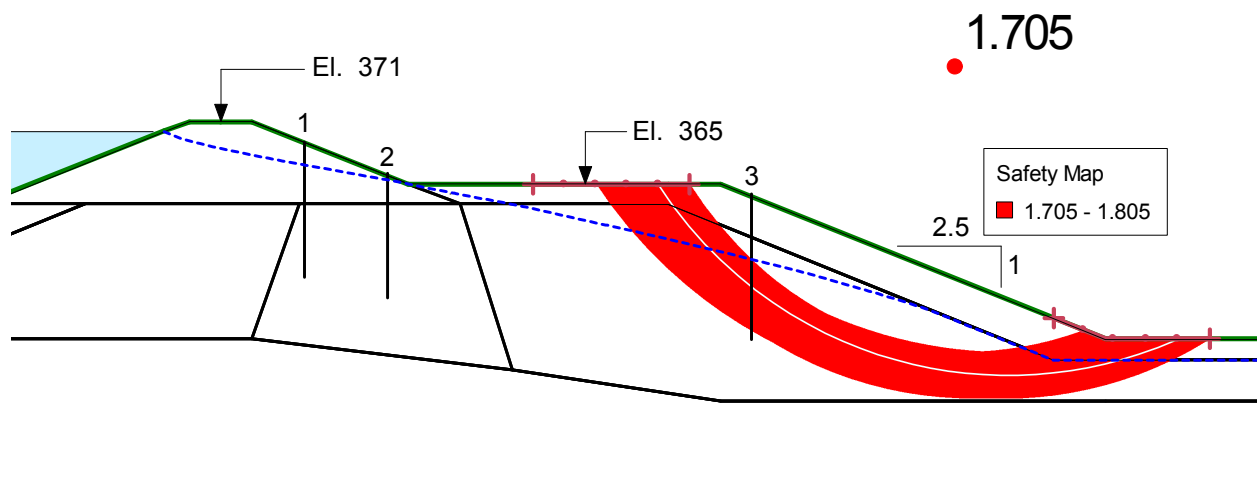


Figure 15 Downstream slope margin of safety before the earthquake

11 Analysis: Earthquake shaking

The next step is to do a dynamic analysis using QUAKE/W. The main purpose of the dynamic analysis is to determine the excess pore-pressures that may develop, and identify zones where the soil may have liquefied or where the soil strength may have dropped down to the steady-state strength.

The QUAKE/W Nonlinear method of analysis is used here. This is an effective stress method, since the pore-pressures that develop during the shaking are used to determine the effective stresses, and the material properties are modified in response to the changing effective stresses.

11.1 Earthquake record

Time history records of the San Fernando earthquake are available from various seismic stations. Most of the past studies have been based on a recording station located on the abutment of the nearby Pacoima Dam, located about 5 km east of San Fernando. The base rock peak acceleration at the San Fernando site has been estimated to be about 0.6 g, and the record is scaled to a maximum 0.6 g to match this value. The time history record used in the analysis here is given in Figure 16. Small vibrations at the start and end of the publicly available record have been removed, limiting the total duration to 14 seconds, which includes all the significant peaks. The data points are presented at a constant 0.01 sec interval.

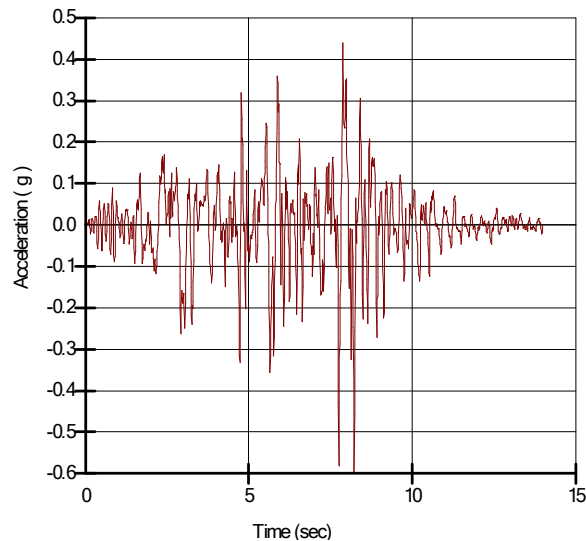


Figure 16 Earthquake record based the station at the Pacoima Dam abutment

11.2 G_{max} moduli

The small strain shear moduli G_{max} are specified as functions. Figure 17 shows the function adopted for the hydraulic fill. The minimum value is 3000 kPa. Functions for the shell material and the alluvium have a similar shape, but with a higher minimum value.

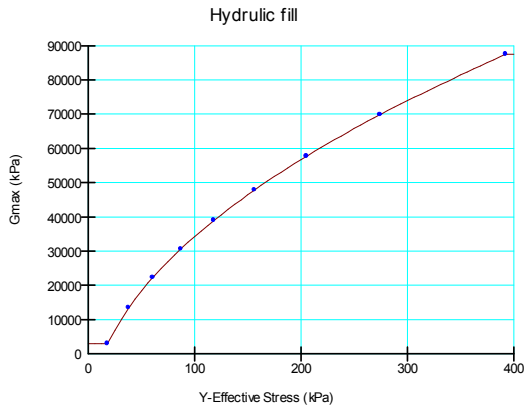


Figure 17 The G_{max} function for the hydraulic fill

12 Pore pressure functions

The Nonlinear Analysis method in QUAKE/W is associated with the MFS (Martin Finn Seed) pore-pressure model. With this model, it is necessary to specify a function such as shown in Figure 18, which defines the volumetric strain that will occur under a given number of cycles for a given shear-strain amplitude. For this analysis, it is specified that the curve in Figure 18 was obtained at shear-strain amplitude of 0.5 percent.

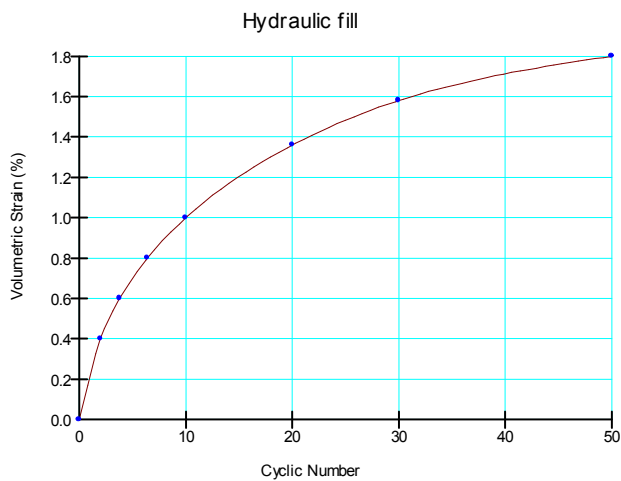


Figure 18 MFS volumetric strain function

The second piece of data required for the MFS pore-pressure model is the Recoverable Modulus function. This is basically the slope of an unloading curve from a one-dimensional odometer test. The curve used in the analysis here is shown in Figure 19.

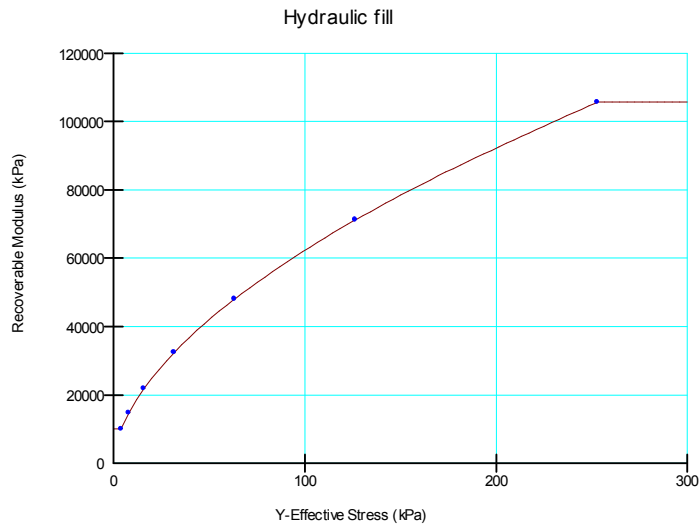


Figure 19 Recoverable modulus function

13 Dynamic response

History Points can be defined at selected points to get a complete picture of the dynamic response; that is, data is saved for each time-step integration point.

Figure 20 shows the response at the crest of the Dam. There is not much difference between this record and the input record in Figure 16. There are a couple of spikes greater than 1g, but outside these spikes the response is more or less a reflection of the earthquake record. In other words, there is no significant amplification or unrealistic damping. This is consistent with the conclusions reached by Seed et al.

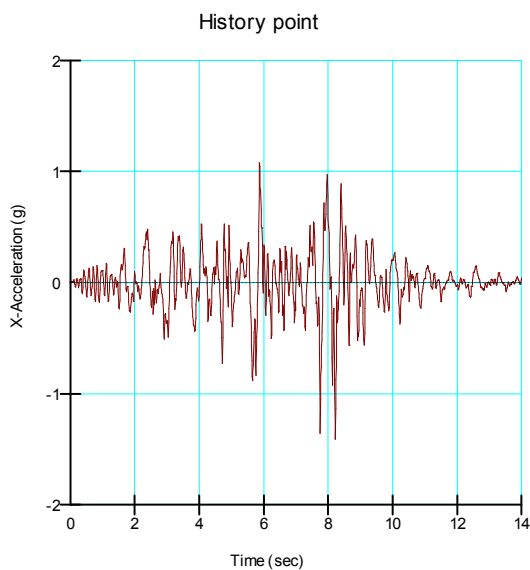


Figure 20 Acceleration versus time at the Dam crest

History Points are also useful for examining the stress-strain response at selected location. A History Point was placed at the base of Piezometer 2. The computed shear stress-shear strain path at this location during the shaking is presented in Figure 21.

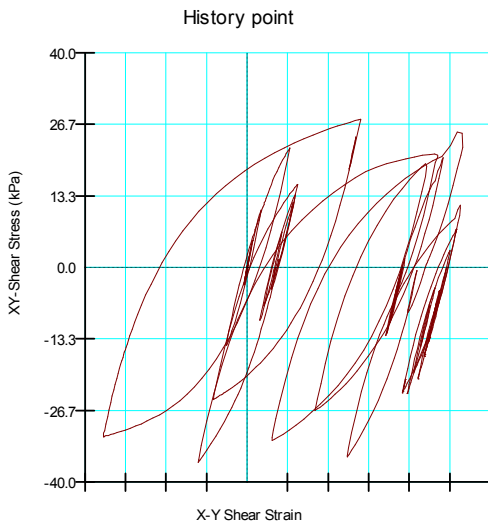


Figure 21 Typical stress-strain path during the shaking

14 Liquefaction

Figure 22 shows contours of q/p' stress ratios under the initial static stresses. A point of significance is the high q/p' ratios in the hydraulic fill underneath the dam crest. This means that there is a zone where the initial q/p' points are near the collapse surface, as discussed earlier in Section 7. The soil strength in this zone could easily fall down to the steady-state strength with a small amount of shaking. There is no yellow shaded area in Figure 23, which indicates that there is zone of initial stress states that are near but still below the collapse surface.

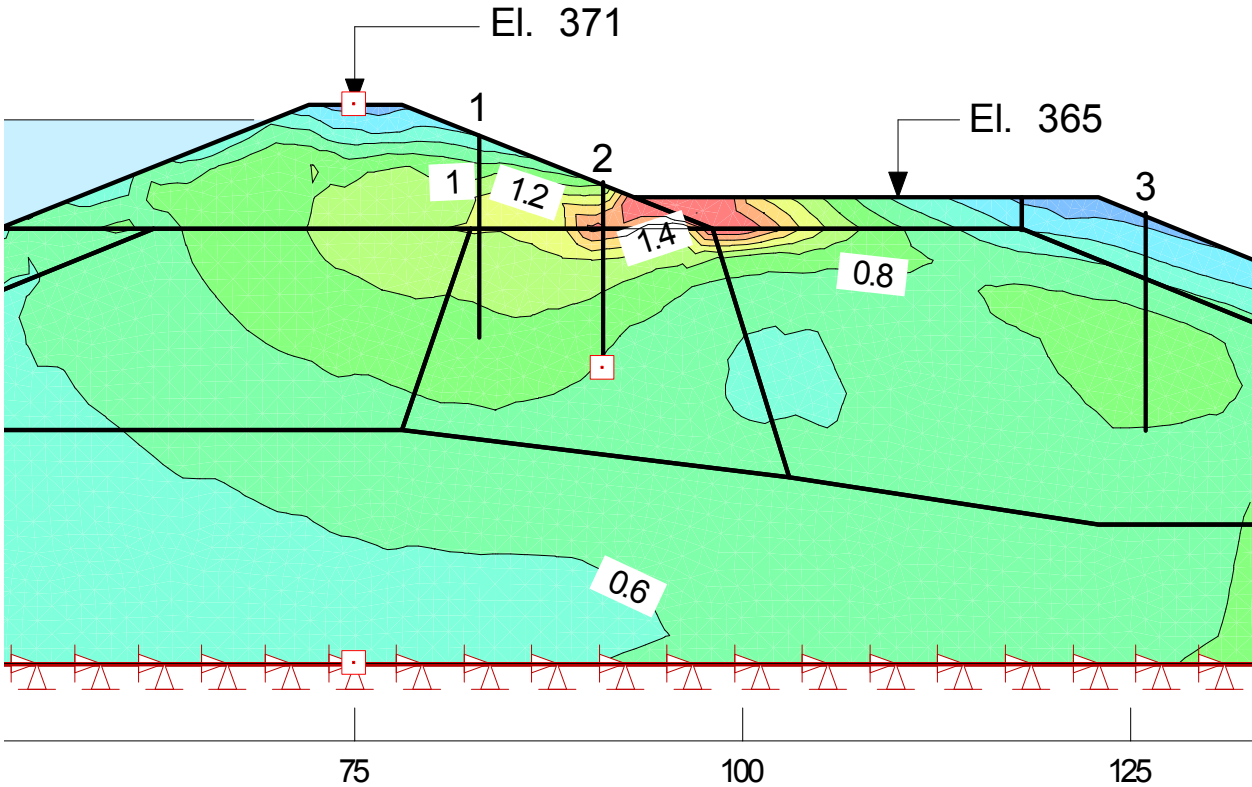


Figure 22 q/p' stress ratios under initial static stresses

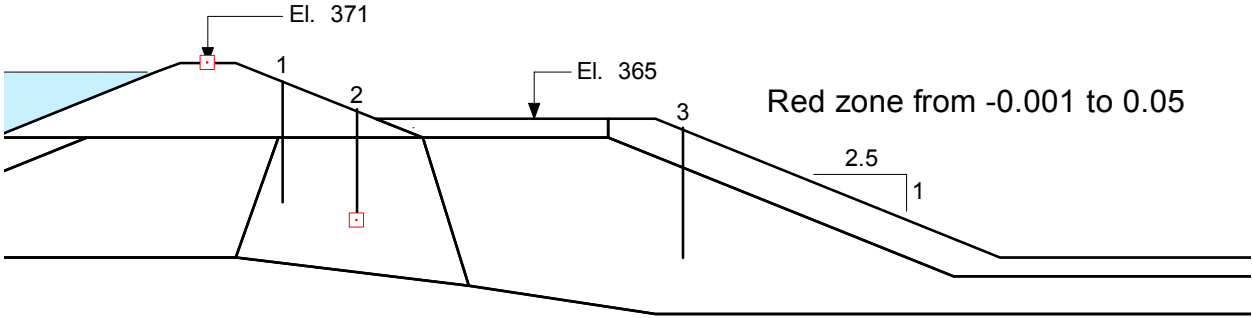


Figure 23 Zone of liquefaction based on initial q/p' stress ratios relative to collapse surface

During the shaking, excess pore-pressures will develop, causing other elements to reach the collapse surface as discussed earlier; in other words, to liquefy. Figure 24 shows the liquefied zone at the end of the shaking.

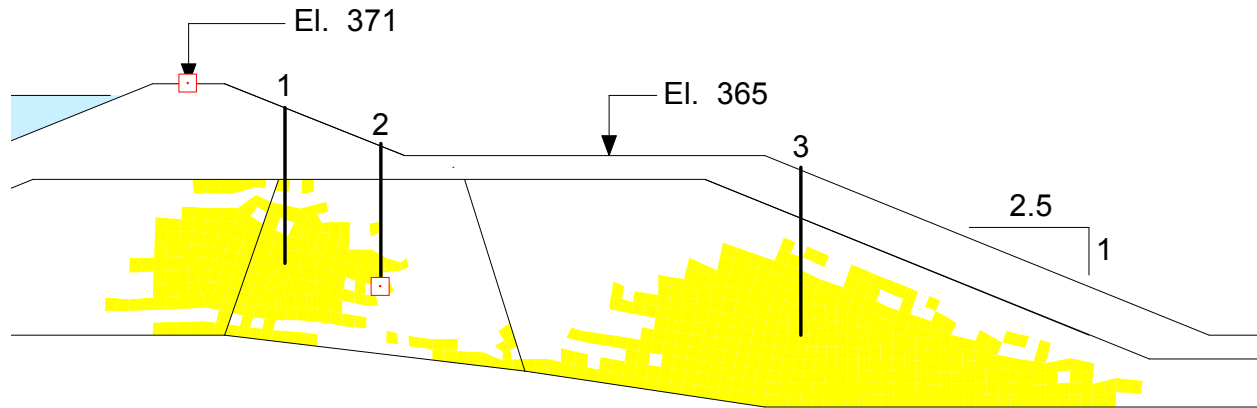


Figure 24 Liquefied zone at the end of shaking.

14.1 Excess pore-pressures

Figure 25 shows contours of the excess pore-pressure at the end of the shaking. The highest excess pore-pressures (90 kPa) are at the bottom of the hydraulic fill below the downstream berm crest.

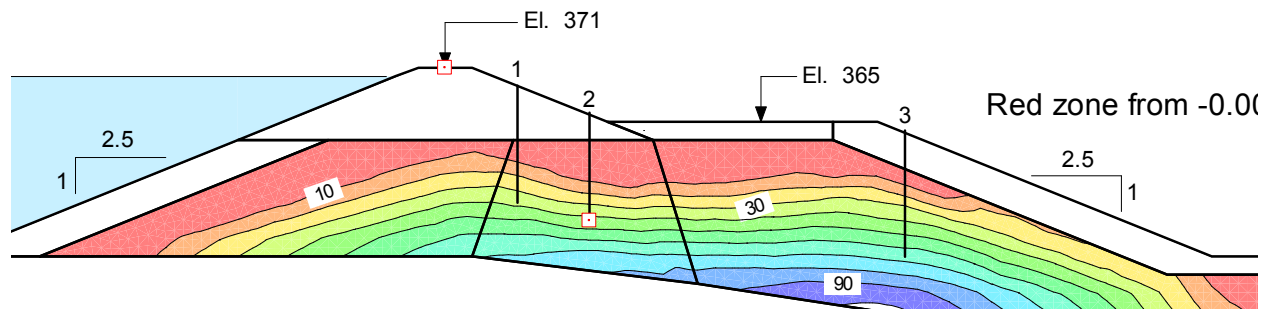


Figure 25 Contours of excess pore-pressure at the end of shaking

Figure 26 shows the build-up of excess pore-pressures at the bottom tip of Piezometer 2. The maximum excess pore-pressure is 43.5 kPa. This is a pressure head of 4.4 m (about 14.5 feet).

The View Results Information command can be used to get the final total H at the base tip of Piezometer 2. The computed H is 369 m. The ground surface at Piezometer 2 is 366 m. The total head H being greater than the ground surface elevation means water would be flowing from the piezometer casing, which is in keeping with observations.

The computer total H at Piezometer 3 is 364 m, and the maximum excess pore-pressure is 66 kPa (6.7 m of pressure head). The elevation at the top of Piezometer 3 is 364. This means that with H equal to 364, the water level in this piezometer would have been at the top of the piezometer. This is higher than what was measured 24 hours after the earthquake. This is consistent with the thinking by Seed et al. that the maximum level was likely higher than what was measured, since some of the excess pore-pressure had already dissipated by the time the reading was taken.

The measured rise in the water level in Piezometer 1 was around 5.2 m (17 feet). The computed total head H at Piezometer 1 is 370 m. The top elevation of the casing is 369 m, meaning that water would flow out of the piezometer, which is in keeping with actual observations.

One of the perplexing issues about Piezometers 1 and 2 is the dramatic difference in the response, even though they are reasonably close together. The sudden rise in Piezometer 1 is about twice that in Piezometer 2. Could it be that cracks formed, and the reservoir water was directly connected to one piezometer and not the other? The analysis cannot provide an answer that question.

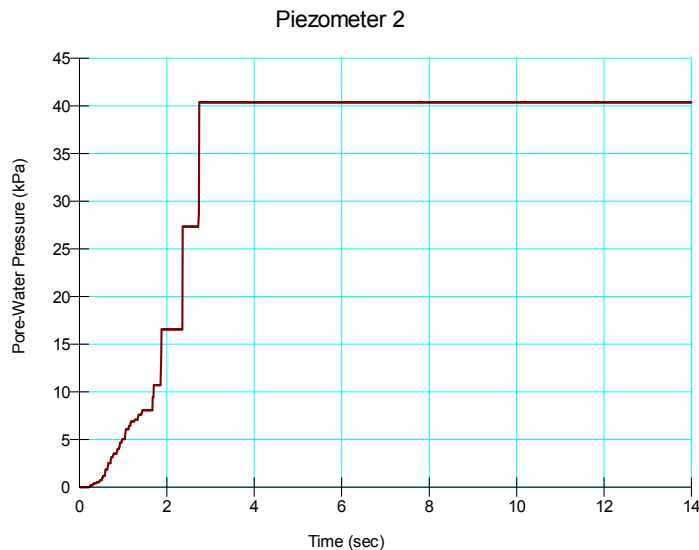


Figure 26 Excess pore-pressure at Piezometer 2

The similarities between the computed and measured responses at Piezometers 1, 2 and 3 provide supporting evidence that the numerical simulation is capturing the trends and tendencies of what actually happened.

15 Post-earthquake stability

SLOPE/W has the capability to use the specified steady-state strength C_{ss} along the portion of a potential slip surface that passes through an element that QUAKE/W has marked as liquefied. Repeating the pre-earthquake stability analysis, but with post-earthquake pore-pressures and with C_{ss} strengths in the liquefied zones, results in factors of safety of close to unity (1.0). Figure 27 shows the situation for the overall stability, and Figure 28, the stability of the downstream slope at the end of the earthquake. In both cases, the low safety factors suggest that the structure was marginally stable at the end of the earthquake, which is intuitively likely.

Figure 29 shows the cohesive strength along the overall critical slip surface. Note how along much of the slip surface, the cohesion is at 35 kPa, which is the specified C_{ss} . Where C_{ss} is 35, ϕ' is zero and therefore the frictional component of the strength is zero.

It is of significant interest that the overall critical slip surface in Figure 27 on the upstream face is exactly in the area where large longitudinal cracks had formed under the reservoir water surface. These cracks only became visible after the reservoir was drawn down, some 12 days after the earthquake.

The safety factor for the overall stability case is 0.923 the steady-state strength is used in the liquefied zones of the dam (Figure 27) as compared to 1.11 using the collapse surface properties ($\phi' = 20$; $C_{ss} = 35$

kPa) and 1.28 using effective stress strength properties ($\phi' = 34$). In the downstream local case, the safety factor is 0.885 if the steady-state strength is used in the liquefied zones of the dam (Figure 28) as compared to 0.978 using the collapse surface properties ($\phi' = 20$; $C_{ss} = 35$ kPa) and 1.054 using effective stress strength properties ($\phi' = 34$). Consequently, it could be argued that in the local downstream case, the C_{ss} strength is not required to explain the observed behavior, but it is certainly required to explain the overall behavior.

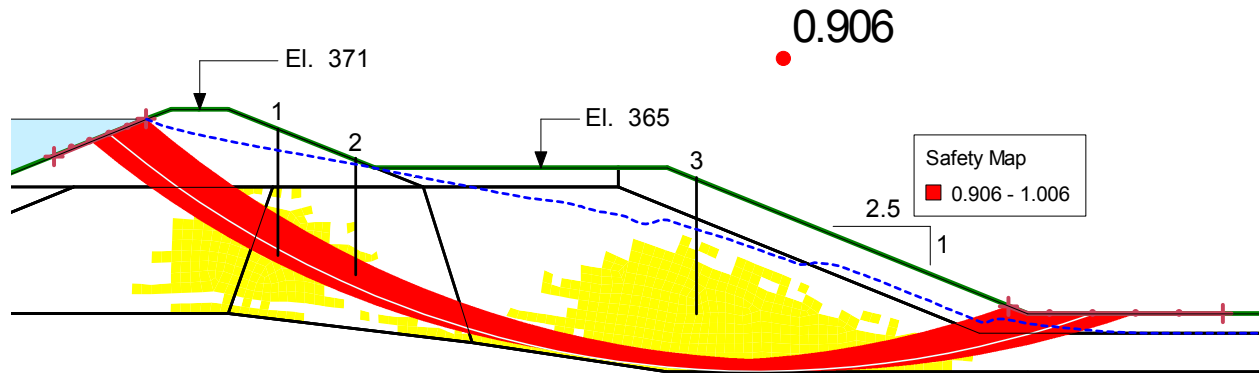


Figure 27 Post-earthquake overall stability

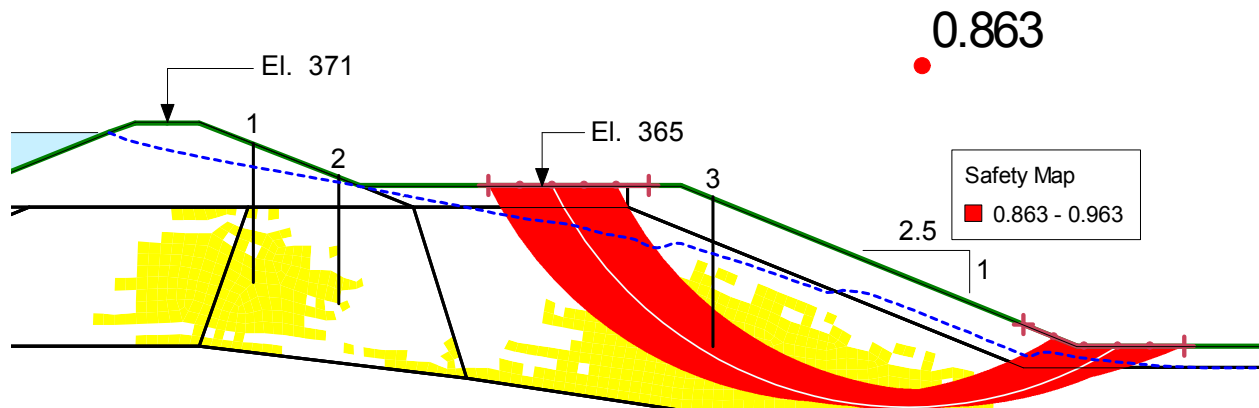


Figure 28 Post-earthquake stability of the downstream slope at the end of the earthquake

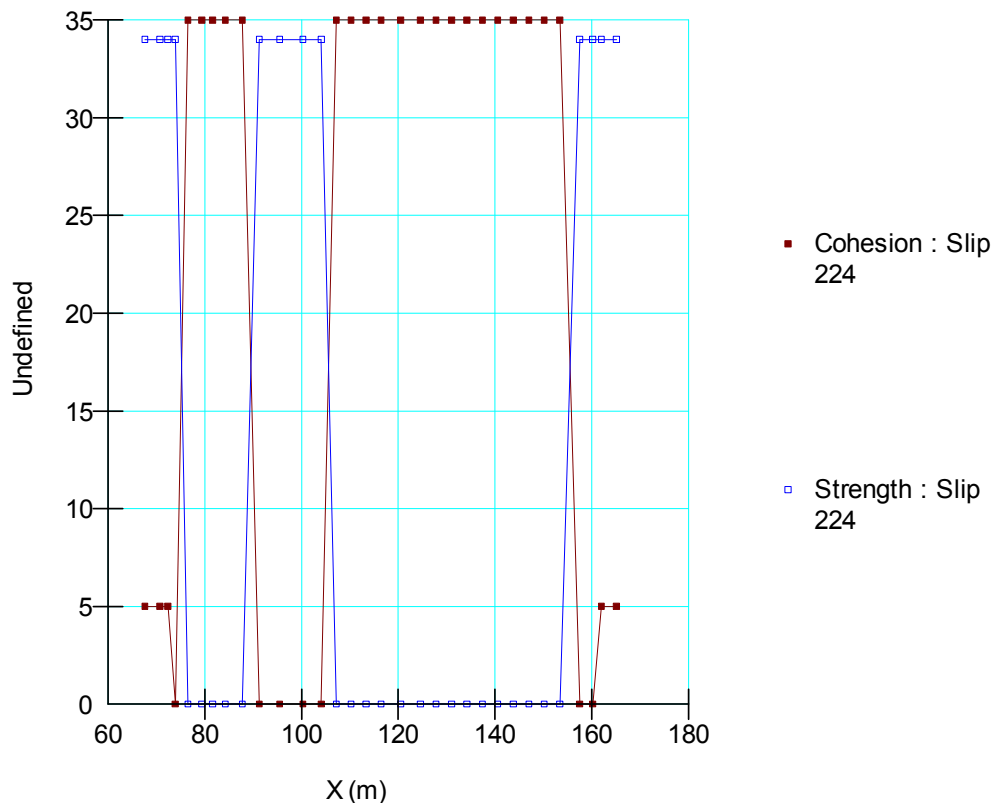


Figure 29 Strength along the overall critical slip surface

16 Post-earthquake deformations

The dam remained marginally stable, but there was some significant permanent displacement, as discussed earlier. Seed et al. came to the view based on field observations that the movements were due to increases in pore-pressures and a corresponding weakening of the soil within a large portion of the dam. The inference is that it was not the inertial forces (mass times acceleration) that were fundamentally at the root of the deformations, but it was the excess pore-pressures and the strength loss.

An estimate of the movements can be made by taking the post-earthquake conditions into SIGMA/W for a stress re-distribution analysis. Some zones were obviously over-stressed after the earthquake due to the strength loss and elevated pore-pressures. The stress re-distribution analysis in SIGMA/W attempts to re-distribute the stresses from the over-stressed zones to other zones that can accept some additional stress before reaching the soil strength. Such a stress re-distribution generally is accompanied with deformations, especially when the overall structure approaches the point of limiting equilibrium. In this case, it has already been shown that the structure was near the point of limiting equilibrium, and a stress re-distribution analysis therefore can provide some information about the failure mechanisms and movements.

Figure 30 shows the displacement vectors from the post-earthquake SIGMA/W stress re-distribution. The movement patterns seem to be a reasonable approximation of what actually happened. The vectors in the upper rolled fill section are down and to the right, and the movement vectors start on the upstream

face in the area where the longitudinal cracks developed. To the right of the upper rolled-fill section, the movement is predominately horizontal, which is also consistent with the observations discussed earlier in Section 5.

There seems to be in part a localized failure on the downstream side. The movements are greater in this area than further upstream. They are distinctly downward at the crest, and lateral and upward at the toe. The strong lateral movements in the toe area are consistent with the pressure ridge that had formed here, the compression failures observed in the outlet conduit and the down slope tipping of the concrete manhole. The movement vectors in general are somewhat characteristic of a localized near circular slip failure.

Generally, the computed movement patterns are entirely consistent with the field observations, and the conclusions arrived at by Seed et al. They concluded that, the *zone of movements within the dam extended vertically over a large portion of the embankment and was not limited to well-defined slip surface at depth*. The computed movement patterns in Figure 30 certainly confirm this.

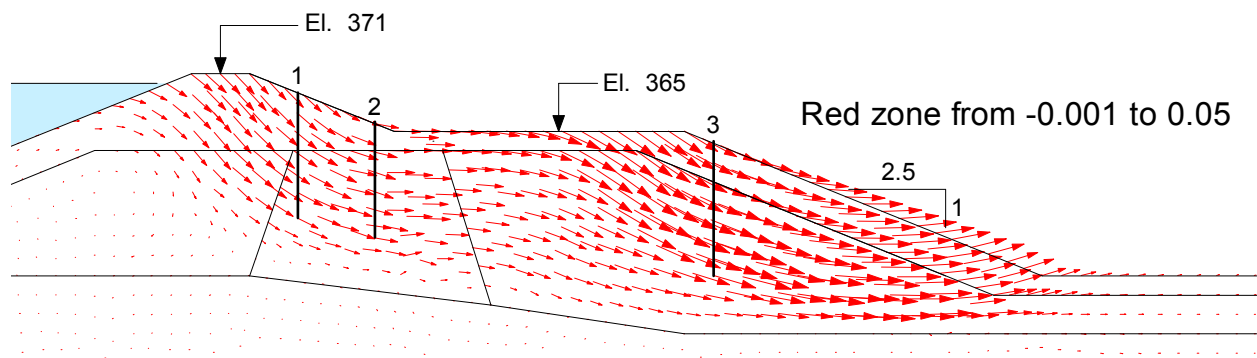


Figure 30 Post-earthquake movement directions

Another way to view the movements is as a deformed section, as in Figure 31. The view gives an appreciation of the down and right movement of the upper rolled fill section and compression bulging in the downstream toe area.

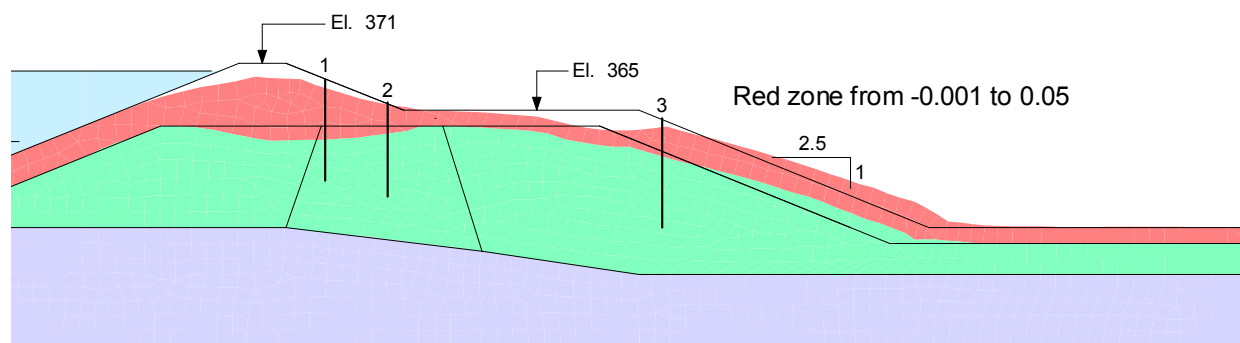


Figure 31 A deformed section at a 10X exaggeration

An interesting result from the stress-redistribution analysis is that there is no tendency for movement in the upstream direction, or any signs suggesting failure in the upstream direction, in spite of the large liquefaction zones shown in Figure 24 under the dam crest and on the upstream side of the crest in the hydraulic fill.

The actual magnitude of the movements is rather difficult to compute with any degree of confidence. When C_{ss} is 35 kPa, the maximum computed movement is less than half a metre. The reported maximum movements at the downstream berm crest are closer to 2 m.

Making an accurate prediction of the permanent displacement is complicated by the fact that the computed displacements are sensitive to the C_{ss} assigned to the liquefied material, and because it is numerically difficult to get a perfectly converged solution from the stress re-distribution analysis when the structure approaches the point of limiting equilibrium. In light of this, any computed movement magnitudes are likely a rough estimate at best.

While it may not be possible to accurately predict the movements associated with a case like this, the analysis exercise can nonetheless be very useful in formulating one's final engineering judgments about the potential behavior of an earth structure like the Upper San Fernando Dam. The trends and mechanisms are every bit as important in evaluating the potential performance of a structure like this as the actual magnitudes of the potential movements.

17 Closing remarks

This analysis of the Lower San Fernando Dam case history clearly demonstrates the advantages of the product integration in GeoStudio. Using QUAKE/W in conjunction with SEEP/W, SIGMA/W and SLOPE/W provides a much clearer picture, than using QUAKE/W in isolation.

This analysis also shows that GeoStudio has all the features required for analyzing the multiple issues inherent in a case like the Upper San Fernando Dam liquefaction failure.

Many of the material properties used in this analysis are simple estimates. They are, however, adequate for understanding the key issues and mechanisms. This is also true for any project. It is good modeling practice to first use realistic estimates of material properties to obtain an understanding of the key issues. Then a decision can be made as to where additional efforts and resources should be spent on further field investigations and testing.

18 References

Castro, G., Seed, R.B., Keller, T.O. Seed, H.B. (1992). *Steady-State Strength Analysis of the Lower San Fernando Dam Slide*, ASCE Journal of Geotechnical engineering, Vol. 118, No. 3, pp. 406-427

Seed, H.B., Lee, K.L., Idriss, I.M. and Makadisi, F.I. (1975). *The Slides in the San Fernando Dams during the Earthquake of February 9, 1971* – ASCE, J of the Geotechnical Engineering Division, GT7, pp. 651-688

Lee, K.L., Seed, H.B., Idriss, I.M., and Makadisi, F.I. (1975). *Properties of Soil in the San Fernando Hydraulic Fill Dams* – ASCE, J of the Geotechnical Engineering Division, GT8, pp. 801-821

Seed, H.B., Idriss, I.M., Lee, K.L. and Makadisi, F.I. (1975). *Dynamic Analysis of the Slide in the Lower San Fernando Dam during the Earthquake of February 9, 1971* – ASCE, J of the Geotechnical Engineering Division, GT9, pp. 889-911